Nicole Anderton* and Michiel Postema

Fragmentation thresholds simulated for antibubbles with various infinitesimal elastic shells

https://doi.org/10.1515/cdbme-2022-1020

Abstract: Antibubbles are small gas bubbles comprising one or multiple liquid or solid cores, typically surrounded by stabilising shells. Acoustically active microscopic antibubbles have been proposed for use as theranostic agents. For clinical applications such as ultrasound-guided drug delivery and flash-echo, it is relevant to know the fragmentation threshold of antibubbles and the influence of the stabilising shells thereon. For antibubbles with an infinitesimal frictionless elastic shell of constant surface tension, we simulated ultrasound-assisted fragmentation by computing radial pulsation as a function of time using an adapted Rayleigh-Plesset equation, and converting the solutions to time-variant kinetic energy of the shell and time-variant surface energy deficit. By repetition over a range of pressure amplitudes, fragmentation thresholds were found for antibubbles of varying size, core volume, shell stiffness, and driving frequency. As backscattering increases with scatterer size, and as drug delivery would require vehicles just small enough to pass through capillaries with a relatively large payload, we chose to present typical results for antibubbles of resting diameter 6 μm with a 90% incompressible core. At a driving frequency of 13 MHz, the fragmentation threshold was found to correspond to a mechanical indices less than 0.4, irrespective of shell stiffness. This mechanical index is not considered unsafe in diagnosis. That means that antibubbles acting as drug-carrying vehicles could release their payload under diagnostic conditions.

Keywords: Acoustic fragmentation, ultrasound contrast agent, shell stiffness, antibubble oscillation modelling, Rayleigh-Plesset equation.

***Corresponding author: Nicole Anderton,** BioMediTech, Faculty of Medicine and Health Technology, Tampere University, Korkeakoulunkatu 3, 33720 Tampere, Finland, e-mail: nicole.anderton@tuni.fi

Michiel Postema, BioMediTech, Faculty of Medicine and Health Technology, Tampere University, Tampere, Finland and School of Electrical and Information Engineering, University of the Witwatersrand, Johannesburg, Braamfontein, South Africa

1 Introduction

Ultrasound contrast agents are used both in diagnosis and therapy, and are therefore referred to as theranostic agents [1]. They comprise microscopic gas bubbles surrounded by stabilising shells [2]. The pulsation dynamics of a spherically symmetric microbubble surrounded by an elastic shell has been modelled with a Rayleigh-Plesset equation, adjusted for the presence of a shell by introducing a shell stiffness parameter [2–5]. Knowing under which conditions ultrasound contrast agent microbubbles fragment might be of interest in echography and ultrasound-guided drug delivery [6, 7]. Shell-encapsulated microbubbles, called parents, subjected to pressures below the inertial cavitation threshold have been observed to typically fragment into eight or more so-called daughter microbubbles [8]. The number of fragments depends on the energy subjected to the parent [8]. The presence of a shell has been found to be of influence on the fragmentation threshold of such microbubbles [7].

Antibubbles are small gas bubbles comprising one or multiple liquid or solid cores [9]. If a surrounding shell is absent, an antibubble is very short-lived [10–12]. The presence of an encapsulating shell or an endoskeleton drastically increases the antibubble lifetime [13–16]. Fluids comprising antibubbles have been proposed for the use as theranostic agents [11, 15, 17, 18].

The dynamic response of microscopic antibubbles by stabilising shells subjected to ultrasound has been studied *in silico* [19, 20], *in vitro* [16, 18, 21], and, more recently, *in vivo* [22]. The simulations and experiments of most of these preliminary studies concentrated on the radial pulsations of antibubbles and the accompanying generation of harmonics. These studies were highly relevant for potential applications of antibubbles in diagnostic harmonic imaging. For potential therapeutic applications of antibubbles, however, it is more relevant to know under which acoustic conditions the core material is released [22]. Ultrasound-assisted disruption of microscopic antibubbles had been demonstrated by high-speed camera footage [21, 22]. From such footage, the fragment size distribution could be predicted [23].

The purpose of this study was to simulate the fragmentation threshold of microscopic antibubbles with infinitesimal

shells of different biomaterial composition. The outcomes of this study may aid in the development of novel theranostic antibubble agents.

2 Methods

An infinite viscous fluid was assumed to surround a perfectly spherical shell-encapsulated antibubble containing one or multiple incompressible cores, subjected to a sound pulse whose wavelength is much greater than the antibubble size. The shell was considered homogeneous, of infinitesimal thickness, elastic, frictionless, and of constant surface tension. For modelling purposes, we replaced the total core volume inside the antibubble by an equivalent core radius. Following a prior derivation [24] but incorporating damping and shell stiffness terms [25], the resulting fundamental pulsation equation used in this study is then given by

$$R\ddot{R}+\tfrac{3}{2}\dot{R}^2=\frac{1}{\rho}\left[\left(p_0-p_\mathrm{v}+\frac{2\sigma R_0}{R_0^2-R_\mathrm{c}^2}\right)\left(\frac{R_0^3-R_\mathrm{c}^3}{R^3-R_\mathrm{c}^3}\right)^{\gamma}+p_\mathrm{v}-\frac{2\sigma R}{R^2-R_\mathrm{c}^2}-2\chi\left(\frac{1}{R_0}-\frac{1}{R}\right)-\frac{4\eta\dot{R}}{R}-\delta\omega\rho R\dot{R}-p_0-p(t)\right]\ , \tag{1}$$

where $p(t)$ is the time-dependent acoustic driving function, p_0 is the ambient pressure, p_v is the vapour pressure, R is the instantaneous radius, R_0 is the initial radius, R_c is the equivalent core radius, γ is the ratio of specific heats, δ is the damping coefficient, η is the liquid viscosity, ρ is the liquid density, σ is the surface tension, χ is the shell stiffness, and ω is the angular driving frequency. The viscous damping had been directly included in (1). Therefore, the damping coefficient δ only comprised the damping owing to reradiation and the thermal damping, $\delta\approx\frac{\omega R}{c}+\frac{3}{5}(\gamma-1)$, where c is the speed of sound of the medium. The angular resonance frequency of a shell-encapsulated antibubble was found by adjusting the resonance frequency of a free-surface antibubble [21] for the surface pressure components in (1) and for the presence of an infinitesimal elastic shell [7]:

$$\omega_\mathrm{r}=\frac{1}{R_0\sqrt{\rho}}\sqrt{\frac{3\gamma\left(p_0-p_\mathrm{v}+\frac{2\sigma R_0}{R_0^2-R_\mathrm{c}^2}\right)}{1-\frac{R_\mathrm{c}{}^3}{R_0^3}}-\frac{2\sigma R_0}{R_0^2-R_\mathrm{c}^2}+\frac{4\eta^2}{R_0^2\rho}+\frac{2\chi}{R_0}}. \tag{2}$$

The fragmentation threshold pressure was defined as the acoustic pressure amplitude at which the kinetic energy of the parent surface [26]

$$E_\mathrm{k}\approx 2\pi\rho R^3\dot{R}^2 \tag{3}$$

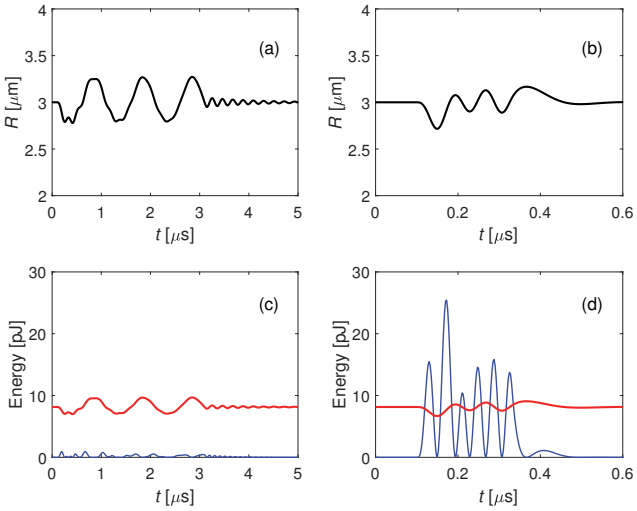

Fig. 1: Radius and instantaneous energies as a function of time simulated for an antibubble of initial radius $R_0=3\,\mu$m with a 90% core radius and shell stiffness $\chi=7.6\,\mathrm{N\,m^{-1}}$ driven with a 0.6-MI pulse of centre frequency 1 MHz (a,c) and 13 MHz (b,d). Instantaneous kinetic energies are indicated by blue lines and surface energy deficits by red lines.

surpassed the difference in surface energy between the parent entity and at least eight daughters [6, 7],

$$\Delta E_\mathrm{s}\approx 4\pi R^2\sigma\ , \tag{4}$$

here referred to as energy deficit.

Numerical solutions of (1) were computed using the `ode45` differential equation solver of MATLAB® (The MathWorks, Inc., Natick, MA, USA). The three-cycle sinoidal acoustic driving function was defined by $p(\omega t)=A\sin\omega t\ \forall\ \omega t\in[0,6\pi]\ \wedge\ p(\omega t)=0\ \forall\ \omega t\notin[0,6\pi]$, in which A was varied to find the fragmentation pressure threshold. The following parameters were chosen in the simulations: $c=1568\,\mathrm{m\,s^{-1}}$, representing saline [27], $p_0=1.00\,\mathrm{atm}$, $p_\mathrm{v}=2.33\,\mathrm{kPa}$, $\gamma=1.4$, $\eta=1.00\,\mathrm{mPa\,s}$, $\rho=998\,\mathrm{kg\,m^{-3}}$, $\sigma=0.072\,\mathrm{N\,m^{-1}}$. Values of R_0, R_c, χ, and ω were variables. Throughout this paper, R_c is expressed as a percentage of R_0. The $R(t)$ curves computed and their time derivatives were converted to kinetic energy and surface energy deficit vectors. Fragmentation pressure thresholds were expressed in mechanical index,

$$\mathrm{MI}=\frac{A\,[\mathrm{MPa}]}{\sqrt{\frac{\omega}{2\pi}\,[\mathrm{MHz}]}}\ , \tag{5}$$

for interpreting the clinical relevance of the findings. An MI$\leq$0.7 is not considered unsafe [28]. Through iteration in MI steps of 0.005, the fragmentation threshold was determined automatically as a function of the variables of choice. The size range was limited to radii small enough to pass through capillaries. The range of shell stiffnesses was limited to those com-

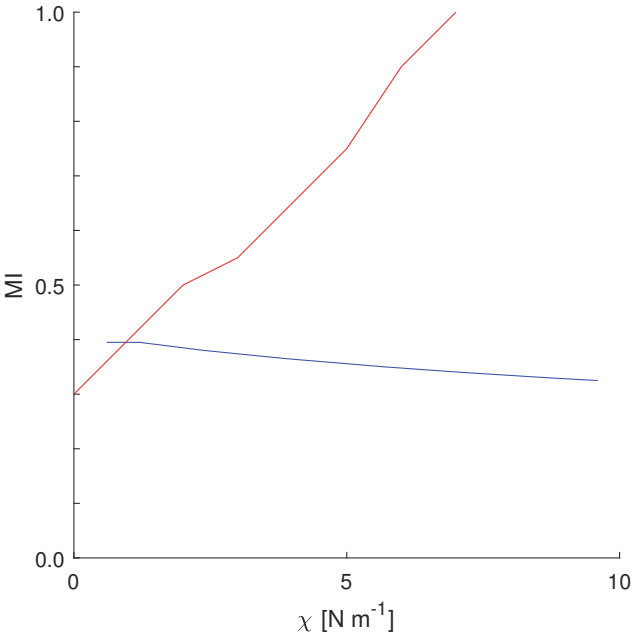

Fig. 2: Fragmentation threshold in MI as a function of shell stiffness χ, simulated for a 3-μm radius antibubble with a 90% core radius, subjected to a pulse of centre frequency 1 MHz (red) and 13 MHz (blue).

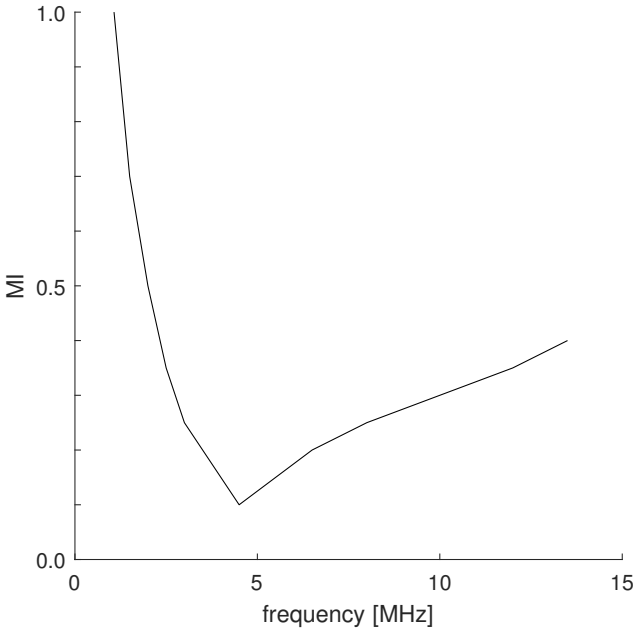

Fig. 3: Fragmentation threshold in MI as a function of driving frequency, simulated for a 3-μm radius antibubble with a 90% core radius and a 7.6-N m^{-1} shell stiffnes.

mon in biomaterials. The frequency range was limited to those common in commercial probes.

3 Results and discussion

Two representative $R(t)$ curves and their corresponding instantaneous energies are shown in Figure 1, for an antibubble of 3-μm initial radius with a 90% core radius, subjected to a 0.6-MI pulse. At a 1-MHz driving frequency, the kinetic energy simulated was too low to cause fragmentation. At a 13-MHz driving frequency, however, the kinetic energy clearly surpassed the surface energy deficit to cause fragmentation.

Figure 2 shows the fragmentation threshold for 3-μm radius antibubbles as a function of shell stiffness at two different sonication frequencies. At a 1-MHz driving frequency, the fragmentation threshold was found to increase with shell stiffness. Here, antibubbles with a shell stiffness less than 7 N m^{-1} were simulated to fragment at an MI$\leq$1. At a 13-MHz driving frequency, however, the fragmentation threshold was found to decrease with shell stiffness. Here, for each stiffness simulated, antibubbles fragmented at an MI$<$0.4. A straightforward explanation of this counterintuitive result is that the resonance frequency of an antibubble increases with its shell stiffness. Consequently, the difference between antibubble resonance and driving frequency may increase or decrease with shell stiffness. The fragmentation threshold should be lowest at resonance. The size of the antibubble core was observed to be only of minor influence on the fragmentation threshold (data not shown).

Figure 3 shows the fragmentation threshold for 3-μm radius antibubbles with shells of 7.6-N m^{-1} stiffness and a 90% equivalent core radius as a function of driving frequency. For driving frequencies greater than 1.5 MHz, the fragmention thresholds corresponded to MI < 0.7. The fragmentation threshold had a minimum of MI = 0.1 at a driving frequency of 4.5 MHz. From (2), it followed that the resonance frequency of such an antibubble is 4.54 MHz. Hence, the driving frequency at the simulated minimum corresponded to the resonance frequency.

Even at a core radius of 90% of the antibubble radius, the fragmentation threshold at 13-MHz driving corresponded to an MI of less than 0.4, which is not considered unsafe in diagnosis. As a consequence, antibubbles acting as drug-carrying vehicles would release their payload under diagnostic conditions.

4 Conclusions

Our simulations show that at lower driving frequencies, the shell stiffness is of major influence on antibubble fragmentation, whilst at higher driving frequencies, the shell mate-

rial is hardly of influence. At 13-MHz driving, stiff-shell-encapsulated antibubbles were simulated to fragment at acoustic amplitudes that are not considered unsafe in diagnosis. These findings imply that drug-loaded antibubbles, stabilised by rigid shells, could be forced to release their contents using diagnostic ultrasound. This research is of interest in flash-echo and ultrasound-guided drug delivery.

Author statement

Research funding: This work was supported by the National Research Foundation of South Africa, Grant Number 127102, and by the Academy of Finland, Grant Number 340026. Conflict of interest: Authors state no conflict of interest. Informed consent: Authors state that informed consent is not applicable. Ethical approval: Authors state that no ethical approval was required for this research as no human or animal samples or data were used.

References

[1] Duan L, Yang L, Jin J, Yang F, Liu D, Hu K, et al. Micro/nanobubble-assisted ultrasound to enhance the EPR effect and potential theranostic applications. Theranostics 2020;10:462–483.

[2] de Jong N, Cornet R, Lancée CT. Higher harmonics of vibrating gas-filled microspheres. Ultrasonics 1994;32:447–453.

[3] Church CC. The effects of an elastic solid surface layer on the radial pulsations of gas bubbles. J Acoust Soc Am 1995;97:1510–1521.

[4] Postema M, de Jong N, Schmitz G. The physics of nanoshelled microbubbles. Biomed Tech 2005;50(S1):748–749.

[5] Mehrem AM. Theoretical study of microbubble dynamics under the action of ultrasound fields. MSc Diss, Universitat Politècnica de València 2013.

[6] Postema M, Schmitz G. Ultrasonic fragmentation of microbubbles: a theoretical approach of the flash in flash-echo. Proc IEEE Eng Med Biol Annu Conf 2005;27:4023–4026.

[7] Postema M, Schmitz G. Ultrasonic bubbles in medicine: influence of the shell. Ultrason Sonochem 2007;14:438–444.

[8] Postema MAB. Medical bubbles. PhD Thesis, University of Twente 2004.

[9] Johansen K, Kotopoulis S, Postema M. Introduction to antibubbles. In: Korneliussen RJ, editor. Proceedings of the 38th Scandinavian Symposium on Physical Acoustics, Geilo 1–4 February 2015. Bergen: CMR; 2015:1–6.

[10] Dorbolo S, Caps H, Vandewalle N. Fluid instabilities in the birth and death of antibubbles. New J Phys 2003;5:161.

[11] Vitry Y, Dorbolo S, Vermant J, Scheid B. Controlling the lifetime of antibubbles. Adv Colloid Interface Sci 2019;270:73–86.

[12] Zou J, Ji C, Yuan BG, Ruan XD, Fu X. Collapse of an antibubble. Phys Rev E 2013;87:061002.

[13] Poortinga AT. Long-lived antibubbles: stable antibubbles through Pickering stabilization. Langmuir 2011;27:2138–2141.

[14] Poortinga AT. Micron-sized antibubbles with tunable stability. Colloids Surf A 2013;419:15–20.

[15] Shen Y, Hu L, Chen W, Xie HH, Fu X. Drop encapsulated in bubble: a new encapsulation structure. Phys Rev Lett 2018;120:054503.

[16] Panfilova A, Chen P, van Sloun RJG, Wijkstra H, Postema M, Poortinga AT, et al. Experimental acoustic characterization of an endoskeletal antibubble contrast agent: first results. Med Phys 2021;48:6765–6780.

[17] Postema M, ten Cate FJ, Schmitz G, de Jong N, van Wamel A. Generation of a droplet inside a microbubble with the aid of an ultrasound contrast agent: first result. Lett Drug Des Discov 2007;4:74–77.

[18] Postema M, Novell A, Sennoga C, Poortinga AT, Bouakaz A. Harmonic response from microscopic antibubbles. Appl Acoust 2018;137:148–150.

[19] Kotopoulis S, Johansen K, Gilja OH, Poortinga AT, Postema M. Acoustically active antibubbles. Acta Phys Pol A 2015;127:99–102.

[20] Johansen K, Postema M. Lagrangian formalism for computing oscillations of spherically symmetric encapsulated acoustic antibubbles. Hydroacoustics 2015;19:197–207.

[21] Kudo N, Uzbekov R, Matsumoto R, Shimizu R, Carlson CS, Anderton N, et al. Asymmetric oscillations of endoskeletal antibubbles. Jpn J Appl Phys 2020;59:SKKE02.

[22] Kotopoulis S, Lam C, Haugse R, Snipstad S, Murvold E, Jouleh T, et al. Formulation and characterisation of drug-loaded antibubbles for image-guided and ultrasound-triggered drug delivery. Ultrason Sonochem 2022;105986.

[23] Anderton N, Carlson CS, Kudo N, Poortinga AT, Postema M. The ultrasound-triggered explosion of an endoskeletal antibubble yields a predictable fragment size distribution. Jpn J Appl Phys 2021;60:128001.

[24] Carlson CS, Matsumoto R, Fushino K, Shinzato M, Kudo N, Postema M. Nucleation threshold of carbon black ultrasound contrast agent. Jpn J Appl Phys 2021;60:SDDA06.

[25] Anderton N, Carlson CS, Matsumoto R, Shimizu R, Poortinga AT, Kudo N, et al. On the rigidity of four hundred Pickering-stabilised microbubbles. Jpn J Appl Phys 2022;61:ac4adc.

[26] Doinikov AA, Dayton PA. Spatio-temporal dynamics of an encapsulated gas bubble in an ultrasound field. J Acoust Soc Am 2006;120:661–669.

[27] Carlson CS, Deroubaix A, Penny C, Postema M. On the attenuation of pure black tattoo ink. SAIEE Afr Res J 2021;112:24–31.

[28] ter Haar G. Safety and bio-effects of ultrasound contrast agents. Med Biol Eng Comput 2009;47:893–900.